On the precipitation behavior of Al-based automotive alloy with low Si content

M.S. Kaiser [iD] [1] [✉], **A.K. Hossain** [iD] [2]

[1] International University of Business Agriculture and Technology, Dhaka, Bangladesh

[2] Bangladesh University of Engineering and Technology, Dhaka, Bangladesh

✉ dkaiser.res@iubat.edu

Abstract. It investigates the function of Si content at lower level on the precipitation behaviour in terms of hardness, resistivity, impedance, X-ray diffraction analysis, differential scanning calorimetry along with structural transformation of Al-based automotive alloys. Conventional metal cast alloys are subsequently allowed to T6 thermal treatment at progression of homogenizing, solutionizing, quenching and ageing. Solution treated samples are aged naturally and artificially, including isochronal and isothermal for different time and temperature. The results suggest that the formation of clusters and GP zones together with metastable phases leads to considerable hardening in aged alloys. As a result, electrical resistivity also increases but decreases at higher ageing temperature for stress relieving followed by metastable phase dissolution and coarsening of fine precipitation. DSC and XRD study confirms the formation of such phases, showing the different peaks. The Si addition entirely changes the precipitation peak of the base alloy for its increasing properties of heterogeneous nucleation and diffusion kinetics in concert with the Si-rich intermetallic. Microstructural observations confirm that solution treatment improves grains distribution and Si additions creates the eutectic phases and coarsens the alloy grain boundaries. Both alloys as well attained more or less entirely re-crystallized after ageing at 350 °C for 60 minutes.
Keywords: Al-alloys; T6 heat treatment; intermetallic; resistivity; activation energy; microstructure

Introduction

The 4xxx series aluminum-silicon alloys have a wide selection of properties used in the manufacture of automobiles, aircraft and electronic components [1,2]. Outstanding castability property, it is suitable for manufacturing of these complex and heavy parts. Binary Al-Si alloys have no special mechanical properties other than castability. To improve the different properties Cu, Ni, Zn, Mg, etc. as minor elements, Ti, Zr, Sc, B, etc. grain refiner and Fe, Pb, Sn impurity elements are also considered into this alloy [3–6]. Common alloying elements Cu and Mg are most of the cases added in this alloy to enhance the higher strength. These two

alloying elements not only improve the strength but also responsive to precipitation hardening of the alloys. To get the superior properties of this Al-Si automotive alloy, Cu well-thought-out 1.0 to 4.0 wt. % and Mg vary from 0.3 to 1.0 wt. % [7,8]. As silicon the major alloying element, so the high strength to weight ratio is the most attractive feature of this alloy. In this Al-Si system, 5 to 23 wt. % Si is used in most of the cases, but the eutectic level is attained at 12.6 wt. % Si [9]. It is well established that Si doping in aluminium alloys increases the fluidity and castabilty, better corrosion resistance, mechanical properties, and machinability. It also forms intermetallics with Mg and other trace elements. As the alloy content different elements, the quantity of the elements presents into the alloys play an important role on every process along with the properties. So, application of heat treatment can change the character and distribution of metallurgical elements in these alloys. The properties of alloys under age-hardening depend entirely on the applied temperature and the duration of the aging process. In the course of ageing process various kinds of coherent aggregates such as solute-rich clusters, GP zones and precipitates can be formed. The presence of these fine intragranular dispersion particles all through the grains promotes high levels of strength of these alloys [10,11].

The investigated work is portion of a general study on precipitation behaviour of Al-Cu-Mg automotive alloy system doped by lower level of Si. Specifically, this investigation involves changes in hardness that occurs during natural and artificial ageing and supplemented by resistivity, impedance, X-ray diffraction (XRD), differential scanning calorimetry (DSC) as well as microstructural study. From the experiment, obtained results will be helpful in future alloy and process development and modelling work of this type of Al-based automotive alloy.

Materials and Methods

Al-based automotive alloys with low level of Si was the most important concern of this study, other than without Si also tried to consider for comparison the property. Commercial purity aluminum, copper and magnesium along with Al-50 wt. %Si master alloy ingot were used to prepare the two experimental alloys. The alloys were cast using a pit furnace of natural gas-fired. Degasser like borax also used for the period of melting in the clay-graphite crucible. The furnace temperature was monitored with the help of Laser Temperature Gun and always maintained the temperature of 750 ± 10 °C. The melt was stirring at 700 °C for homogenizing and then poured into 250 °C preheated mild steel mould of 20 × 200 × 300 in millimeter. The chemical compositions of both alloys, obtained by Shimadzu PDA 700 optical emission spectrometer, are as follows in Table 1.

Table 1. By wt% average chemical composition from OES analysis

|	Si	Cu	Mg	Fe	Ni	Pb	Zn	Mn	Ti	Al
Alloy 1	0.244	2.158	0.767	0.211	0.199	0.163	0.076	0.065	0.005	Bal
Alloy 2	3.539	2.309	0.784	0.273	0.217	0.166	0.083	0.067	0.010	Bal

First, the oxide layer of the cast alloy surfaces was removed by machining and then allowed to hold in a muffle furnace at 450 °C for 12 h for homogenization. To obtain a supersaturated single-phase region of the alloys, the samples were then solutionized at 535 °C for 2 h followed by rapid quenching in salt water. For the ageing study, the thermally treated alloys were pieced of 18 × 18 × 5 in mm. The samples were subjected to natural ageing for more than two months. Artificial ageing conducted as isochronal for 60 minutes up to 350 °C and isothermal at 200 °C for 30–360 minutes. Following this, the finished surface of the samples was produced by polishing for this measurement. Automatic Turret Micro Vickers Hardness Tester, model: HV-1000DT was used for measuring the microhardness of the different processes aged samples and this time 1 Kg load for 10 seconds was applied with the Knoop indenter. Fifteen indentations were taken from different positions on every finish

sample and the average value was considered. The electrical resistivity of the alloys was determined using a Type 979, electrical conductivity meter, calculated from that electrical conductivity data.

The experiment of differential scanning calorimetry was done under inert N_2 gas atmosphere using DSC131 EVO Analyser. The samples weight was a lump of 34 mg. The test was conducted with scan rate of 10 °C/min from room temperature to 600 ºC. The activation energy was calculated through the DSC heating run of the alloys using Nagasaki–Maesono analysis [12]. The X-ray diffraction analysis of the aged samples was done using a PHILIPS PW1830 diffractometer with Cu-Kα (0.154 nm) radiation. The operating voltage for all the diffraction analysis was 45KV and the tube current was 35 MA respectively. The diffraction angle scan rate was 10/mm and step used 0.02 in the range of 25 to 90 ºC. At room temperature, LCR meter and Impedance Analyzer were used for the AC electrical measurements where the considered range of 100 Hz $\leq$ f $\leq$ 100 MHz. A 10 × 8 × 3 mm finish surface was prepared for this study. For the metallographic studies, the heat-treated samples were polished with alumina, etched with Keller's reagent and observed under a Versamet-II Microscope. SEM of the aged samples was carried out by a Jeol Scanning Electron Microscope type of JSM-5200 with X-ray analyzer to verify the different elements present in the experimental alloys.

Results and Discussion

Age-hardening behavior. Natural ageing. Figure 1 shows the change in average microhardness of the solution treated base Alloy 1 and 3.5 %Si added Alloy 2 during natural ageing condition. It is clear that both alloys gain some degree of hardness within 65 days of natural aging. It is postulated that during natural ageing, the solute atoms form clusters or co-clusters of Mg, Si and Cu. Such clusters are supposed to hinder the free movement of dislocations as a result of an increase in hardness. However, the Si added alloy initially shows higher hardness because of different alloying elements with Si are re-dissolved for producing a solute-rich homogeneous solid solution. Higher formation of Si clusters accelerates the ageing response of 3.5 %Si added alloy. Except it Si also refines the grain structure, so the hardness improved as stated by the Hall-Petch equation [13,14]. A decrease in hardness is observed for both alloys after a few days, which can be attributed to the relieving of internal stresses due to casting and solution treatment. It is slightly higher for Si added alloys, as higher foreign particles cause higher internal stress.
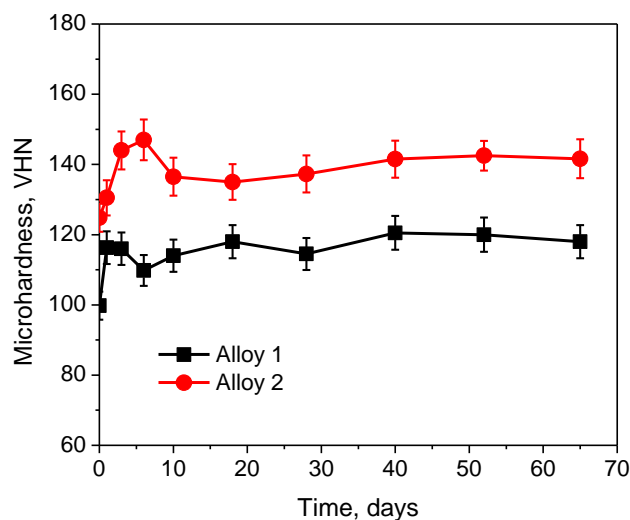
Fig. 1. Natural ageing behavior of two experimental alloys for 65 days

Artificial ageing. Isochronal ageing. The effect of isochronal ageing for one hour on the micro-hardness of the alloys is plotted in Fig. 2. The curves associated with hardness exhibit the twice ageing peaks during the entire aging period. But Si added Alloy 2 shifts the hardness peaks in terms of intensity and temperature than that of base Alloy 1. The first precipitates, formed during the aging process, are usually linked with atomic clusters, and GP zones form rapidly in the Al matrix. These precipitates are very fine and coherent with the matrix of Al, and thus cause a strong strengthening effect by inhibiting dislocation movement. A further metastable phase is formed following the aging process which is semi-coherence with the matrix and can efficiently oppose the movement of dislocations, so creating some reinforcing effect. The age-hardening effect between the two peaks is less for both alloys. During this aging period, the GP zones dissolve to form metastable phases. Hence, the level of GP zones for dissolution is considerably reduced, and metastable precipitates are not formed since then. So it is effectively damaged to prevent dislocation movement. Such alloys exhibit double aging peaks, as reported in earlier investigations [10,15]. Additionally, during aging solution treated Alloy 1 follow the precipitation sequence formation of atomic clusters, GP zones, homogeneous intermediate phase θ''-Al_2Cu, heterogeneous intermetallic phase θ'-Al_2Cu and equilibrium phase θ-Al_2Cu. Alloy 2 doped with Si produces supplementary intermediate β''-Mg_2Si phase, heterogeneous precipitation of β'-Mg_2Si and rod or plate-shaped equilibrium β-Mg_2Si phase. The utmost strength of the alloy is attained immediately prior to the precipitation of incoherent θ and, β-platelets. The S-$CuAlMg_2$ phases may be formed in case of Alloy 1 and Si-link precipitates as Q-$Al_5Cu_2Mg_8Si_6$, π-$Al_9FeMg_3Si_5$ and β-Al_5FeSi etc. for Alloy 2, but this has a minor contribution in strength than the θ' and β' phases [16].
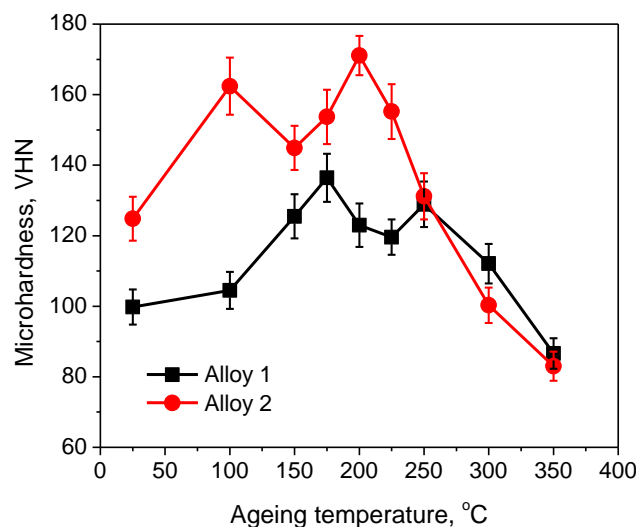

Fig. 2. Microhardness changes of two experimental alloys under isochronal ageing treatment

However, significant evidence shows that Si addition not only extends the age hardening intensity but also provide an earlier aging response. These experiences can be attributed to the Si-phase having a great control over the diffusion behavior of Cu in the Al-matrix. The nucleation as well as the growth process of θ' (Al_2Cu) take place earlier because of the heterogeneously nucleation, this contributes to amplify the aging kinetics and superior strength via the early aging. In addition, it is associated with higher diffusion rates of Si and Mg elements compared to Cu [17,18]. Si doped alloy leads to the formation of Si-rich precipitates as responsible for the high strength. At the final aging stage, a sharp decline in the hardness of alloys is observed. This is obvious, the over ageing effect on the alloys. Metastable strengthening precipitates become coarser and grain growth occurs faster, resulting in transformation of even stable incoherent precipitates, which are inefficient in

limiting dislocation motion. Another point to note is that the alloy with Si addition at higher aging temperature shows lower hardness since higher diffusion rate of Si.

The changes of the average values of electrical resistivity with the aging temperature of the experimental alloys is put on show in Fig. 3. The early fall in resistivity during ageing is related to stress relieving of the alloys. The transition materials attach the vacancies into the alloy strongly. Therefore, the concentration of scattering centers decreases, hence the resistivity drop off. The following increase in resistivity is due to formation of fine intermetallic precipitates. The sharp fall in electrical resistivity of the alloys is associated with recovery of strain and dissolution of metastable phases already present in the alloy matrix. The initial resistivity of solution treated Alloy 2 containing 3.5 Si shows higher values than base Alloy 1 due to higher Si-rich intermetallic in the alloy. During ageing higher amount of Si forms different intermetallic with different elements, dissolution also occurs as a result some variations are there. Dissolution of β precipitate and hence strain recovery is the factor responsible for the above drop in resistivity [15,19]. These resistivity values depend on two things, as the GP zone and various precipitation formations increase the resistivity and stress relieving and recovery decrease the resistivity of the alloys. So the sum of these results is displayed in the graph. The Si added alloy demonstrates the higher rate of decreasing because of higher stress reliving behaviour as it contents the higher fraction of intermetallic in solid solution. Alloys with Si addition at intermediate stages also show signs of early precipitation peaks.
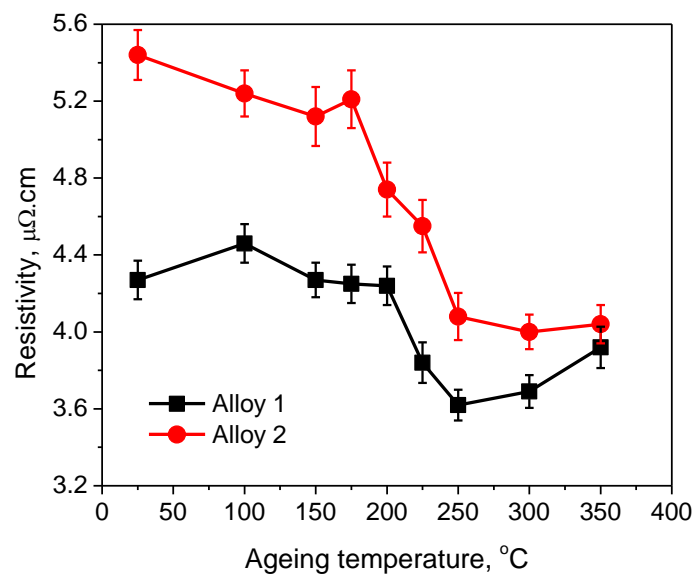
Fig. 3. Electrical resistivity changes of the two alloys under isochronal ageing treatment

Isothermal ageing. Figures 4 and 5 show the values of average hardness and the resistivity of the alloys when aged isothermally at 200°C for varying timelines. For both, the alloys first increases with ageing time due to fine high density GP zones formation which have the capacity to strengthen, and then the hardness decreased due to dissolution of GP zone (Fig. 4). As the GP zone dissolves, the precipitates then grow to a stable phase, which has a relatively weak strengthening effect. Following this, a subsequent strengthening effects are observed as associated with nanoscale metastable precipitates [20]. Ageing for a long time, the hardness decreases due to continuously precipitates coarsening and even start

transforming to stable θ precipitate. In case of Si doped alloy, early aging reaction is visible due to increase in nucleation characteristics [18].
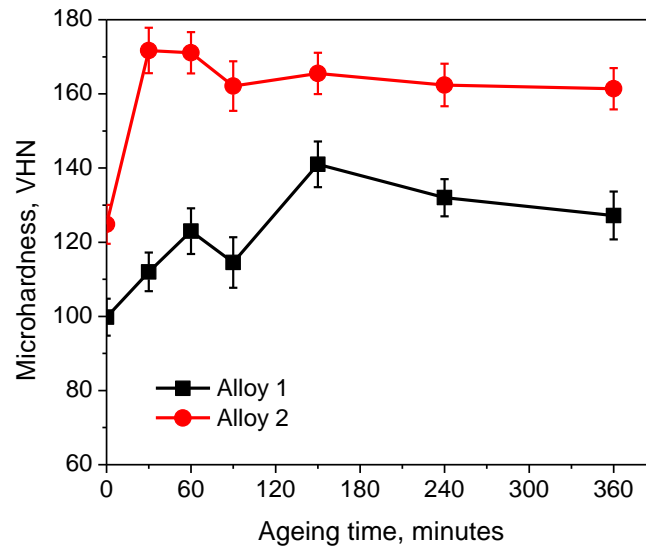
Fig. 4. Microhardness changes of the two alloys under isothermal ageing treatment

Both alloys exhibit a general trend of decreasing of resistivity with aging time (Fig. 5). However, Si added Alloy 2 at early stage of aging offers a higher reduction in resistivity compared to base Alloy 1. It is already point out that GP zone and different precipitation formation increase the resistivity of the alloys, and stress reliving and recovery decrease the resistivity of the alloys. So the summation of these results is displayed in the graph. At extend ageing time, the decrease of resistivity fully related with precipitation and grain coarsening of the alloys. Fine precipitates make the alloy defects which obstruct the electron movement and coarsen precipitates losses the efficiency, hence the higher and lower resistivity [15].
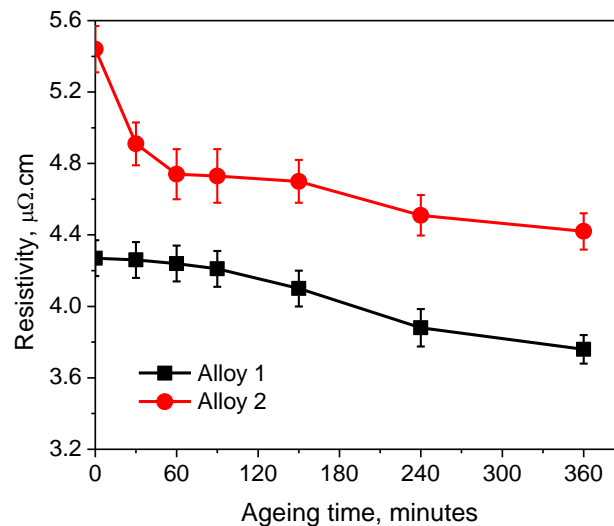
Fig. 5. Resistivity changes of two alloys under isothermal ageing treatment

Impedance behavior. At room temperature, the frequency dependence impedance behaviour of Al-based automotive alloys are plotted in Fig. 6. It is observed that both solutions treated alloys exhibited higher impedance at low frequencies and decreases with the higher frequency. According to Drude Lorentz model, capacitive effects are higher at low frequencies because there are scattering effects of electrons colliding with the lattice as well

as electric polarization of bound electrons not in the conduction band. A number of interfacial polarization may be occurred. At lower frequencies it leads to high impedance because grouping of both effects capacitive and purely resistive [21]. The graph also demonstrated that 3.5Si added Alloy 2 attain the higher impedance followed the base Alloy 1. The impedance properties of any material depend on different factors. These are microstructural defects like porosity, microcracks, dislocations, vacancies, along with impurities, dopant atoms etc. Normally, addition of impurities significantly increases the impedance characteristics of the metal.
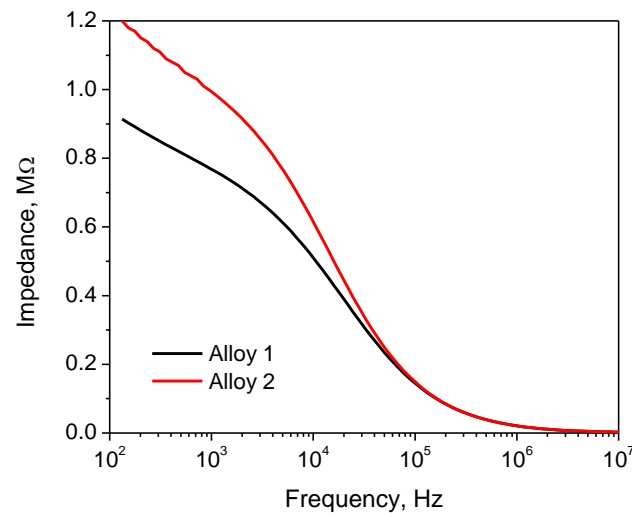
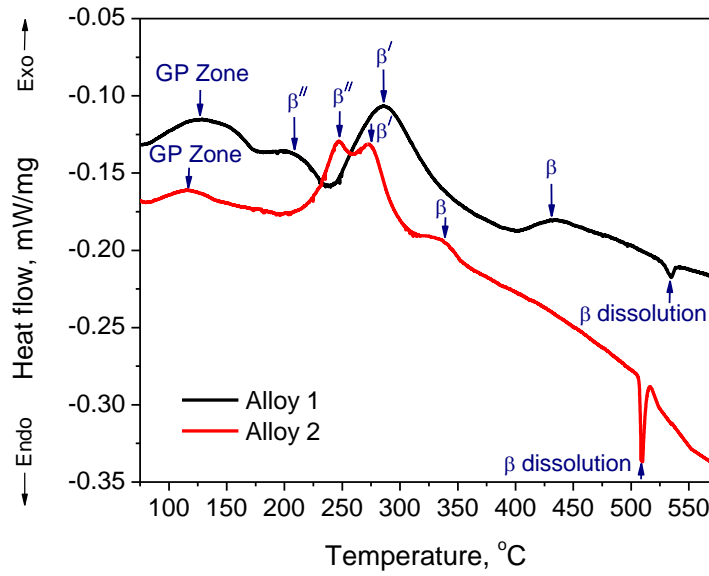**Fig. 6.** Comparison of impedance behaviour of both alloys with applied frequency

Thermal analysis. Figure 7 represents the DSC heating curve of both alloys at solution treated condition. Two alloys each consists of the similar number of four exothermic and one endothermic peak, but the happening temperatures are different. Four consecutive exothermic peaks indicative formation of GP zones, β'' phase, β' phase and β phase followed the endothermic peak corresponds to the dissolution of β phase. It may be supposed that dissolution of previous phases occurs only to form a later phase [22,23].

From Fig. 7 along with Table 2, it is put on show for Alloy 1 that GP zones form at 130 °C with an activation energy 64 kJ/mol of the process. But corresponding to Alloy 2, it occurs earlier as at 115 °C and 60 kJ/mol respectively. It is inferred that Si added alloy forms Mg_2Si phases which perform as heterogeneous nucleation site for formation of Al_2Cu and Si phase subsequently devoid of any particular crystal orientation. As a result, the peak occurs earlier along with lower process activation energy. Similarly, for Alloy 1, the activation energy of the heterogeneous precipitation β' and stable equilibrium phase β phase are calculated as 283 and 203 kJ/mol, corresponding temperature at 285 and 435 °C respectively whereas Alloy 2 demonstrate at 265 and 185 kJ/mol at 273 and 335 °C. Intermediate β'' phase for Alloy 1 forms at 205 °C with an activation energy of 115 kJ/mol, other than Alloy 2 form this phase at 247 °C with 126 kJ/mol activation energy [24]. Intermediate phase occurs homogeneous as a result no symptom of early on. Again, the lastly endothermic peak in course of heating associated with dissolution of stable β phase, form at 534 °C with an activation energy of 240 kJ/mol for Alloy 1 and a sharper exothermic peak at 510 °C with an activation energy of 222 kJ/mol for Alloy 2. Similar nature is observed earlier regarding the occurrence of the peak. In case of dissolution of β phase, there is a tendency to occupy the Cu atoms by blocky Al_2Cu and not dissolved in Al matrix easily, so the higher both values. The diffusion rates of Si and Mg elements are higher compare to Cu as a result earlier formation of dissolution peak with lower activation energy of the Si doped alloy [18].

Table 2. Results of DSC study

Alloy	Transformation	Peak temperature (°C)	Activation energy (kJ/mol)
Alloy 1	GP zone	130	64
	β″ phase	205	115
	β′ phase	285	283
	β phase	435	203
	Dissolution of β phase	534	240
Alloy 2	GP zone	115	60
	β″ phase	247	126
	β′ phase	273	265
	β phase	335	185
	Dissolution of β phase	510	222

Fig. 7. DSC heating curve of the solution treated two alloys
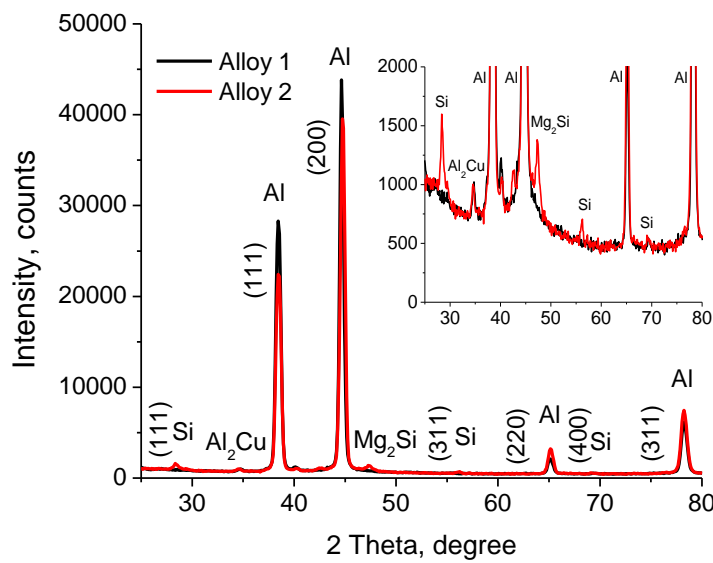
Fig. 8. XRD patterns of two alloys ageing treated at 200 °C for 150 minutes

The XRD data analysis of both alloys at T6 heat-treated state is presented in Fig. 8. The base Alloy 1 shows the peak Al phase along with the Al_2Cu. As the silicon is doped, additionally Alloy 2 creates the peak of the silicon phase Mg_2Si. It is also noted that Alloy 2 produces the Si peaks and reduces the level of Al, resulting in a decrease in the peak position of Al compared to Alloy 1. These two intermetallics play the important role on the strengthening of the alloys as stated earlier. At the T6 heat treatment condition other peaks are not clearly observed, as the associated intermetallics are in an extremely narrow range, which is untraceable by X-ray analysis [25].

Optical microscopy. After solution heat treatment at 535 °C for 2 h, the microstructure of the tested alloys are shown in Fig. 9 to illustrate the effect of Si. The microstructure of base Alloy 1 consists mainly of primary Al dendrites with minor elements like Cu, Mg, Fe in solid solution (Fig. 9(a)). These are consistently spread into Al-matrix since the solidification under fast cooling [26]. Silicon added by 3.5 wt. % Alloy 2, to some extent, refines the microstructure and coarsens the grain boundaries (Fig. 9(b)). The microstructure also displays eutectic silicon clearly fragmented with more spherical.
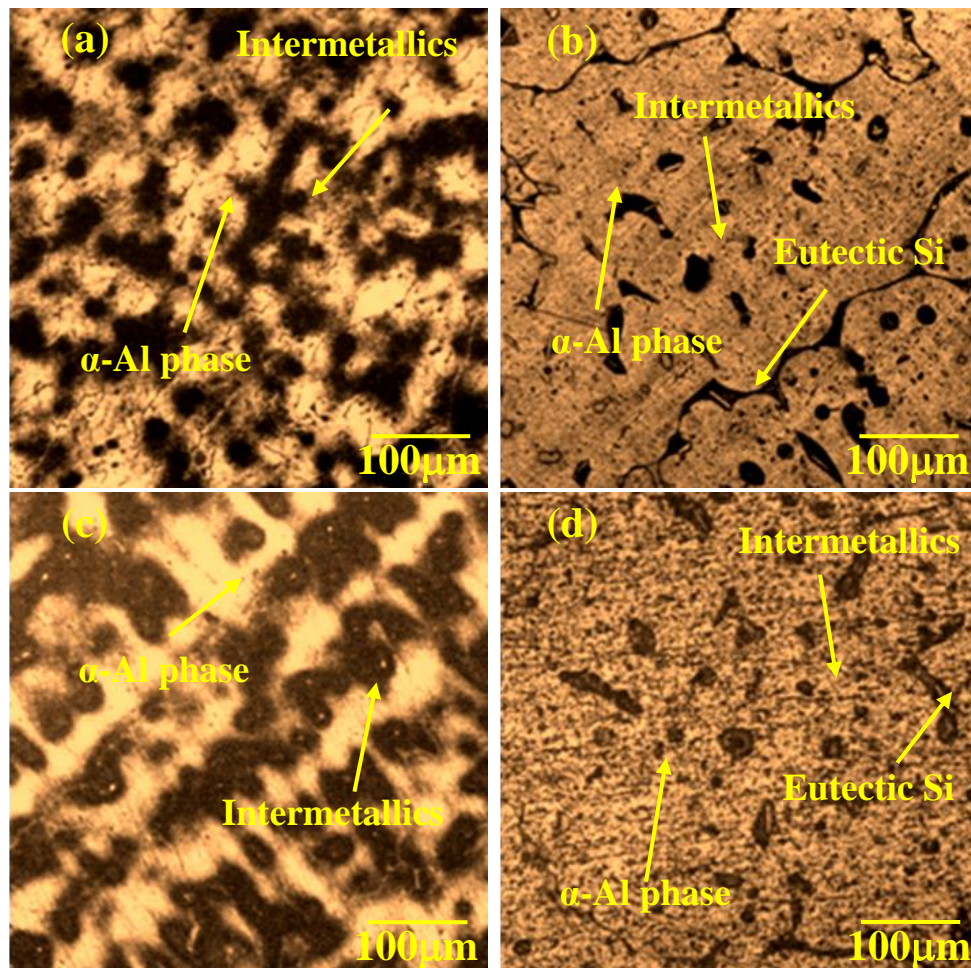

Fig. 9. Solution treated microstructures (a) Alloy 1, (b) Alloy 2 and ageing treated at 350 °C for 60 minutes (c) Alloy 1, (d) Alloy 2

After an ageing treatment at 350 °C for a timeline of one hour, both alloy microstructures are found to be more or less entirely recrystallized (Fig. 9(c,d)). Dendrites appear to be dissolved as well as precipitates coarsening occurred that are uniformly distributed in the matrix [27]. Consequently, the microstructure consists of equiaxed grains. Whereas the microstructure background is not very clear as the prior solution treated alloys.

This is due to the presence of intermetallic aggregates in growth α-Al phase of the base alloys. Moreover, for alloy containing Si, the elongated Si particles are well seen in the microstructure diffused from the aluminium matrix as it does not dissolve in this ageing condition.

      Scanning electron microscopy. SEM micrographs along with EDS spectra of the two alloys in Fig. 10 are performed to complement the optical microstructural studies. The typical micrographs are in T6 heat-treated condition as solutionizing, rapid cooling and then aged at 200 °C for 150 minutes. No symptom of crystallization in the microstructure of the two alloys is observed at these ageing conditions. As usual in base Alloy 1 exists various intermetallic particles uniformly distributed in the α-Al phase and at grain boundaries also (Fig. 10(a)). When Si is doped by 3.5 wt. % Alloy 2, a number of rough as well as elongated eutectic phases turn to visible, which separate the alloy α-Al matrix (Fig. 10(b)). These plate-like eutectic Si distributes at the grain boundaries, causing coarsening of the grain boundaries [15,28]. The corresponding EDX of the SEM indicate the following elements by wt. % in Alloy 1, 97.28 %Al, 0.03 %Si, 1.94 %Cu, 0.64 %Mg, 0.05 %Fe and 0.06 %Ni similarly Alloy 2 are 92.08 %Al, 4.81 %Si, 2.26 %Cu, 0.57 %Mg, 0.15 %Fe and 0.13 %Zn. The results obtained from the analysis satisfy the elements composition of the experimental alloys, as presented in Table 1.
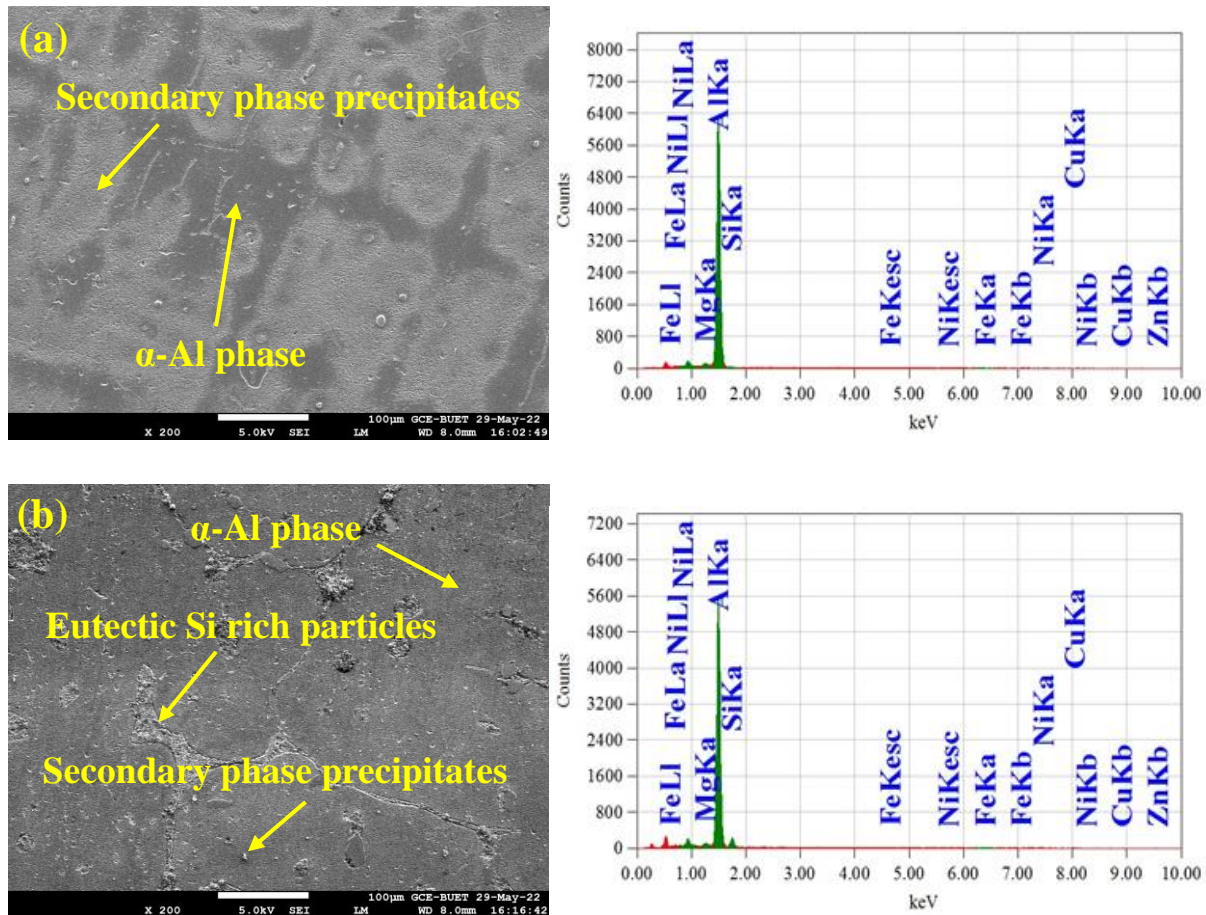
Fig. 10. SEM images of (a) automotive base Alloy 1 and (b) 3.5Si added Alloy 2 ageing treated at 200°C for 150 minutes

Conclusions

The precipitation behavior of low Si doped Al-based automotive alloys is addressed and conclusions can be drawn based on the above investigations:

1. Two consecutive hardening peaks are generated in both the aged alloys. Ageing sequence consists of different phases, but GP zones and the metastable phases are associated to these ageing peaks. The main strengthening phases are θ-Al_2Cu, β-Mg_2Si and Q-$Al_5Cu_2Mg_8Si_6$. The Si rich intermetallics make the difference of strengthening properties when Si is alloyed to this alloy. Adding up of Si showed earlier ageing peaks with higher intensities by its increasing properties of heterogeneous nucleation and diffusion kinetics. The optimum hardness of the alloys can be achieved after aging around at 200 °C for 150 minutes.

2. Electrical resistivity of the alloy increases with Si addition to form the higher Si-rich intermetallics along with others that hinder the movement of electrons and phonons. But it increases throughout ageing for precipitates formation and decrease due to internal stress relieving, metastable phase dissolution and the precipitates coarsening in to the alloys.

The addition of silicon led to more degree of eutectic silicon in the alloy microstructure and makes the grain boundary coarsen. Ageing at 350 °C for 60 minutes, the alloys attain the fully re-crystallized state and consist of equiaxed grains.

References

1. Polmear J. *Light Alloys-Metallurgy of the Light Metals*. 3rd. ed. Arnold; UK; 1995.

2. Zhou P, Wang D, Nagaumi H, Wang R, Zhang X, Li X, Zhang H, Zhang B. Microstructural Evolution and Mechanical Properties of Al-Si-Mg-Cu Cast Alloys with Different Cu Contents. *Metals*. 2023;13(1): 1–13.

3. Khalikova GR, Zakirova GR, Farkhutdinov AI, Korznikova EA, Trifonov VG. Surface hardening of an Al-Si-Cu-Ni-Mg aluminum alloy by friction stir processing and T6 heat treatment. *Letters on Materials*. 2022;12(3): 255–260.

4. Gutkin MY, Skiba NV, Orlova TS. Grain-boundary nanoprecipitates-mediated mechanism of strengthening in Al-Cu-Zr alloy structured by high-pressure torsion. *Materials Physics and Mechanics*. 2022;50(3): 431–438.

5. Park SI, Han SZ, Choi SK, Lee HM. Phase equilibria of Al3(Ti, V, Zr) intermetallic system. *Scripta Mater*. 1996;34(11): 1697–1704.

6. Kaiser MS, Basher MR, Kurny ASW. Effect of scandium on microstructure and mechanical properties of cast Al-Si-Mg alloy. *J. Mater. Eng. Perform*. 2012;21(7): 1504–1508.

7. Davis JR. *ASM Specially Handbook, Aluminum and Aluminum alloys*. OH, USA: ASM International; 1993.

8. Chen F, Liu C, Zuo L, Wu Z, He Y, Dong K, Li G, He W. Effect of thermal exposure on mechanical properties of Al-Si-Cu-Ni-Mg aluminum alloy. *Crystals*. 2023;13(236): 1–12.

9. Biswas P, Patra S, Roy H, Tiwary CS, Paliwal M, Mondal MK. Effect of Mn addition on the mechanical properties of Al-12.6Si alloy: Role of Al15(MnFe)3Si2 intermetallic and microstructure modification. *Met. Mater. Int*. 2021;27: 1713–1727.

10. Toschi S. Optimization of A354 Al-Si-Cu-Mg alloy heat treatment: effect on microstructure, hardness, and tensile properties of peak aged and overaged alloy. *Metals*. 2018;8(11): 1–16.

11. Kaiser MS. Solution treatment effect on tensile, impact and fracture behaviour of trace Zr added Al-12Si-1Mg-1Cu piston alloy. *Journal of the Institution of Engineers (India): Series D*. 2018;99(1): 109–114.

12. Nagasaki S, Maesono A. High Temp. High Press. *Metals Physics*. 1965;11: 182.

13. Ding L, Jia Z, Zhang Z, Sanders RE, Liu Q, Yang G. The natural aging and precipitation hardening behaviour of Al-Mg-Si-Cu alloys with different Mg/Si ratios and Cu additions. *Mater. Sci. Eng. A*. 2015;627: 119–126.

14. Ghassemali E, Riestra M, Bogdanoff T, Kumar BS, Seifeddine S. Hall-Petch equation in a hypoeutectic Al-Si cast alloy: grain size vs. secondary dendrite arm spacing. *Procedia Eng.* 2017;207: 19–24.

15. Kaiser MS. Effect of solution treatment on the age-hardening behavior of Al-12Si-1Mg-1Cu piston alloy with trace-Zr addition. *J. Cast. Mater. Eng.* 2018;2(2): 30-37.

16. Mao H, Bai X, Song F, Song Y, Jia Z, Xu H, Wang Y. Effect of Cd on Mechanical Properties of Al-Si-Cu-Mg Alloys under Different Multi-Stage Solution Heat Treatment, *Materials.* 2022;15(15): 1–14.

17. Vo NQ, Dunand DC, Seidman DN. Role of silicon in the precipitation kinetics of dilute Al-Sc-Er-Zr alloys. *Mater. Sci. Eng. A.* 2016;677: 485–495.

18. Mohamed AMA, Samuel FH. *A review on the heat treatment of Al-Si-Cu/Mg casting alloys.* London, UK: IntechOpen; 2012.

19. Junho OP, Noronha MML, Mello SRS, Oliveira CD. Relationship between Electrical Conductivity and the Stage of the Heat Treatments of Aging and Overaging of the Aluminum Alloy AA2024. *Mater. Sci. Forum.* 2018;930: 400–404.

20. Abdelaziz MH, Elgallad EM, Doty HW, Samuel FH. Strengthening precipitates and mechanical performance of Al-Si-Cu-Mg cast alloys containing transition elements. *Mater. Sci. Eng. A.* 2021:820: 1–8.

21. Kaiser MS. Effect of trace impurities on the thermoelectric properties of commercially pure aluminum. *Materials Physics and Mechanics.* 2021;47(1): 582–591.

22. Hamdi I, Boumerzoug Z, Chabane F. Study of precipitation kinetics of an Al-Mg-Si alloy using differential scanning calorimetry. *Acta Metall. Slovaca.* 2017;23(2): 155-160.

23. Chen Z, Liu K, Elgallad E, Breton F, Chen XG. Differential scanning calorimetry fingerprints of various heat-treatment tempers of different aluminum alloys. *Metals.* 2020;10(6): 763.

24. Liu M, Wu Z, Yang R, Wei J, Yu Y, Skaret PC, Roven HJ. DSC analyses of static and dynamic precipitation of an Al-Mg-Si-Cu aluminum alloy. *Prog. Nat. Sci.: Mater. Int.* 2015;25(2): 153–158.

25. Ahn SS, Pathan S, Koo JM, Baeg CH, Jeong CU, Son HT, Kim YH, Lee KH, Hong SJ. Enhancement of the mechanical properties in Al-Si-Cu-Fe-Mg alloys with various processing parameters. *Materials.* 2018;11(11): 2150.

26. Liu K, Cao X, Chen XG. Effect of Mn, Si, and cooling rate on the formation of iron-rich intermetallics in 206 Al-Cu cast alloys. *Metall. Mater. Trans. B.* 2012;43(5): 1231–1240.

27. Liu M, Wada T, Suzuki A, Takata N, Kobashi M, Kato M. Effect of annealing on anisotropic tensile properties of Al-12%Si alloy fabricated by laser powder bed fusion. *Crystals.* 2020;10(11): 1007.

28. Li L, Zheng Y, Chen Y, Feng J, Li C, Chen L, Zuo L, Zhang Y. Study on microstructure distribution of Al-Cu-Mg alloy in squeeze casting process. *J. Phys. Conf. Ser.* 2022;2338: 012038.

THE AUTHORS

Mohammad Salim Kaiser (iD)
e-mail: dkaiser.res@iubat.edu

Al-Kabir Hossain (iD)
e-mail: 1610161@me.buet.ac.bd